Lab on a Chip

PAPER

View Article Online
View Journal | View Issue

Cite this: *Lab Chip*, 2021, **21**, 2050

Coupling fluid flow to hydrogel fluidic devices with reversible "pop-it" connections†

Reha Abbasi, [ab] Thomas B. LeFevre, [ab] Aaron D. Benjamin,[ac] Isaak J. Thornton [ac] and James N. Wilking [*ab]

Received 21st February 2021,
Accepted 15th March 2021

DOI: 10.1039/d1lc00135c

rsc.li/loc

Hydrogels are soft, water-based polymer gels that are increasingly used to fabricate free-standing fluidic devices for tissue and biological engineering applications. For many of these applications, pressurized liquid must be driven through the hydrogel device. To couple pressurized liquid to a hydrogel device, a common approach is to insert tubing into a hole in the gel; however, this usually results in leakage and expulsion of the tubing, and other options for coupling pressurized liquid to hydrogels remain limited. Here, we describe a simple coupling approach where microfluidic tubing is inserted into a plastic, 3D-printed bulb-shaped connector, which "pops" into a 3D-printed socket in the gel. By systematically varying the dimensions of the connector relative to those of the socket entrance, we find an optimal head-socket ratio that provides maximum resistance to leakage and expulsion. The resulting connection can withstand liquid pressures on the order of several kilopascals, three orders of magnitude greater than traditional, connector-free approaches. We also show that two-sided connectors can be used to link multiple hydrogels to one another to build complex, reconfigurable hydrogel systems from modular components. We demonstrate the potential usefulness of these connectors by established long-term nutrient flow through a 3D-printed hydrogel device containing bacteria. The simple coupling approach outlined here will enable a variety of applications in hydrogel fluidics.

Introduction

Hydrogels are soft, water-based polymer gels[1–4] with widespread applications in medicine[5,6] and bioengineering.[7,8] While hydrogels have long been incorporated into fluidic devices,[9,10] the development of stand-alone hydrogel fluidic devices and other hydrogel fluidic elements with complex three-dimensional structures has historically been limited. However, recent advances in rapid fabrication are now enabling the creation of hydrogel-based fluidic elements and free-standing devices with complex, high-resolution structures.[11–14] For example, hydrogel-based photoreactors,[15] bioreactors,[16] and a variety of engineered tissues with intricate structures[17–20] and microscale vasculature[11,15,16,20–24] have been created. As rapid fabrication technologies continue to advance, the use of hydrogel-based fluidic devices are expected to expand.[25]

To drive liquid through a fluidic device, tubing containing liquid must be coupled to the device. For devices composed of hydrogel, this presents a challenge.[25] A common solution, used in soft polydimethylsiloxane (PDMS)-based microfluidics, is to simply insert microfluidic tubing into a hole in the device.[26,27] In a PDMS device, static friction between the tubing and PDMS prevents the tubing from slipping out of the device and allows the formation of a robust, high-pressure seal.[28] However, when this approach is attempted with hydrogel devices, a thin layer of water on the surface of the gel lubricates the interaction between the gel and tubing and allows the tubing to slip out under relatively low pressure. Adhesives and barb-type connectors have been shown to provide stable, high-pressure seals,[29] but simple, reversible connector solutions are still needed, and the lack of such technologies limits the development of hydrogel-based fluidics.

Here, we describe a simple, reversible, plug-based connector designed to couple microfluidic tubing to a hydrogel-based fluidic device, to allow for pressurized liquid flow through the system. The connection consists of a 3D-printed plastic plug inserted into a matching spherical socket in a 3D-printed hydrogel, which is then held in place by the elasticity of the gel. We call this a "pop-it" connector. The connection can easily be removed and reinserted, allows for rotation around the long axis of the connector, and can also be used to link individual

[a] *Center for Biofilm Engineering, Montana State University, 214 Roberts Hall, Bozeman, MT, 59717, USA. E-mail: james.wilking@montana.edu*
[b] *Chemical and Biological Engineering Department, Montana State University, 214 Roberts Hall, Bozeman, MT, 59717, USA*
[c] *Mechanical and Industrial Engineering Department, Montana State University, 214 Roberts Hall, Bozeman, MT, 59717, USA*

† Electronic supplementary information (ESI) available. See DOI: 10.1039/d1lc00135c

hydrogel modules to one another to build complex, reconfigurable fluidic hydrogel systems. To characterize the connection, we systematically vary the diameter of the connector head relative to the diameter of the gel socket entrance, measure both the force required for insertion and the liquid pressure the resulting seal can withstand, and find the head-socket ratio that provides the maximum resistance to leakage and expulsion. To demonstrate the usefulness of these connectors, we use them to deliver nutrient broth to a 3D printed hydrogel containing bacteria for over a day. The simple and robust connector design should enable a variety of hydrogel fluidic applications.

Results & discussion

To illustrate the standard approach for driving liquid into soft microfluidic devices, we create a cylindrical, mm-scale hole in a PDMS-based microfluidic device using a biopsy punch and insert plastic tubing into the hole (Fig. 1A). The outer diameter of the tubing (OD = 1.09 mm) is larger than the inner diameter of the hole (ID = 0.65 mm) and is held in place by static friction. This friction is enough to withstand the pressure needed to drive liquids through the device, which can approach $\Delta P \approx 10^3$ Pa.[30,31]

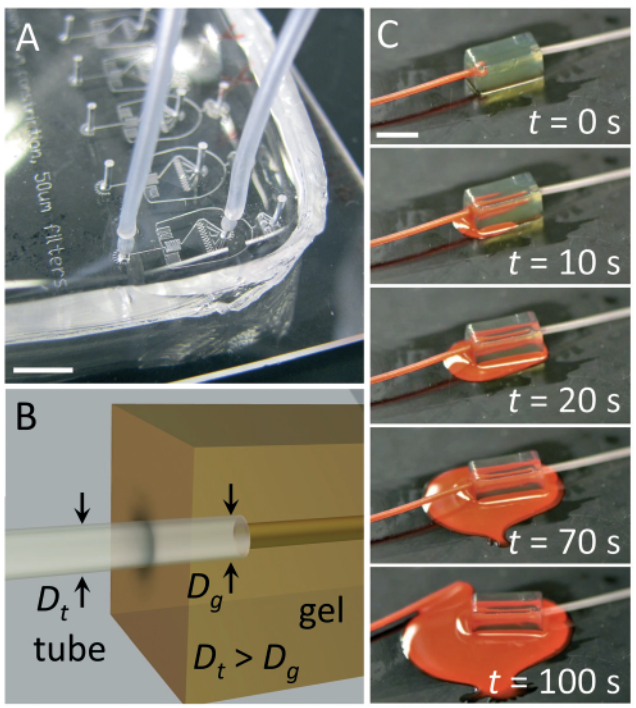

Fig. 1 Friction-based connections developed for traditional microfluidic devices fail when applied to hydrogels. (A) Liquid is introduced into a soft microfluidic device by punching a hole in the PDMS and inserting larger diameter microfluidic tubing into the hole. Static friction prevents the tubing from being expelled even for liquid pressures as high as $\Delta P \approx 10^3$ Pa. When the same approach is applied to a 3D printed PEG-DA hydrogel, where (B) tubing is inserted into a smaller diameter hole in the surface of the gel to a depth of 3 mm, (C) the tubing is expelled from the hydrogel as liquid is forced into the gel at low pressure ($\Delta P \approx 1$ Pa). Scale bars in (A) and (C) correspond to 5 mm and 10 mm, respectively.

By contrast, when tubing is inserted into a hydrogel fluidic device, friction between the tubing and gel is insufficient to resist even very small pressures. To demonstrate this, we 3D print a cm-scale polyethylene glycol diacrylate (PEG-DA) hydrogel (10 w/w%) containing a single straight channel of length, l = 12 mm and diameter, D = 0.8 mm and insert microfluidic tubing into the channel. The outer diameter of the tubing (OD = 1.32 mm) is larger than the inner diameter of the channel entrance (ID = 1.20 mm) corresponding to a gel strain of $\gamma \approx 0.1$, so the gel exerts a radial compressive stress on the tubing (Fig. 1B). When we drive water through the hydrogel using a syringe pump at a low flow rate (Q = 200 μL min^{-1}), we observe that the seal begins to leak in less than 10 seconds, and the tubing, with an inserted section length, $l \approx 3$ mm, is forced out of the hydrogel in less than 100 seconds. This is illustrated by the series of time-resolved images in Fig. 1B. While the failure rate depends on a variety of factors such as gel elasticity, surface moisture, surface roughness, and gel strain, leakage and tubing expulsion from hydrogel-based fluidic devices occurs consistently and at low flow rates. Failure occurs even more frequently when hydrogels with smaller channels and more complex vasculature are used due to the higher pressures required to drive flow.

To address this issue, we design and fabricate a plastic connector and gel socket pair that serves to secure fluidic tubing to the hydrogel. Our connector is plug-shaped, and 3D printed using a photopolymerizable plastic (see Methods). Microfluidic tubing is inserted into the connector and the two are held together with static friction (Fig. 2A). To couple the tubing and connector assembly to a hydrogel, a matching socket is printed at the channel inlet to the hydrogel, and the connector is inserted into the socket, as shown in Fig. 2B and C. The design is such that a lip of gel at the channel orifice is stretched during connector insertion and relaxes to form a tight seal around the connector after insertion. We call this a "pop-it" connection. These connectors are simple and easy to manufacture. For example, the batch of connectors shown in Fig. 2D ($n \approx 100$) can be fabricated in less than two hours. A hydrogel with pop-it connectors inserted on both inlet and outlet ports is shown in the photograph in Fig. 2E.

Provided a connector is matched with a smaller-diameter, appropriately sized gel socket, the gel will form a seal and the elasticity of the gel will resist removal. Appropriate sizing is based on the condition that the head of the connector, with diameter D_c, is larger than the inner neck diameter D_g of the gel socket ($D_c/D_g > 1$; Fig. 2B and C). Intuitively, we expect the seal to improve as D_c/D_g increases; however, if D_c/D_g is too large, the gel will fracture during connector insertion. To determine the magnitude of the forces associated with connector insertion as well as the largest achievable D_c/D_g ratio without gel fracture, we systematically vary D_c/D_g and for each condition measure the force required for insertion as well as the maximum liquid pressure the seal

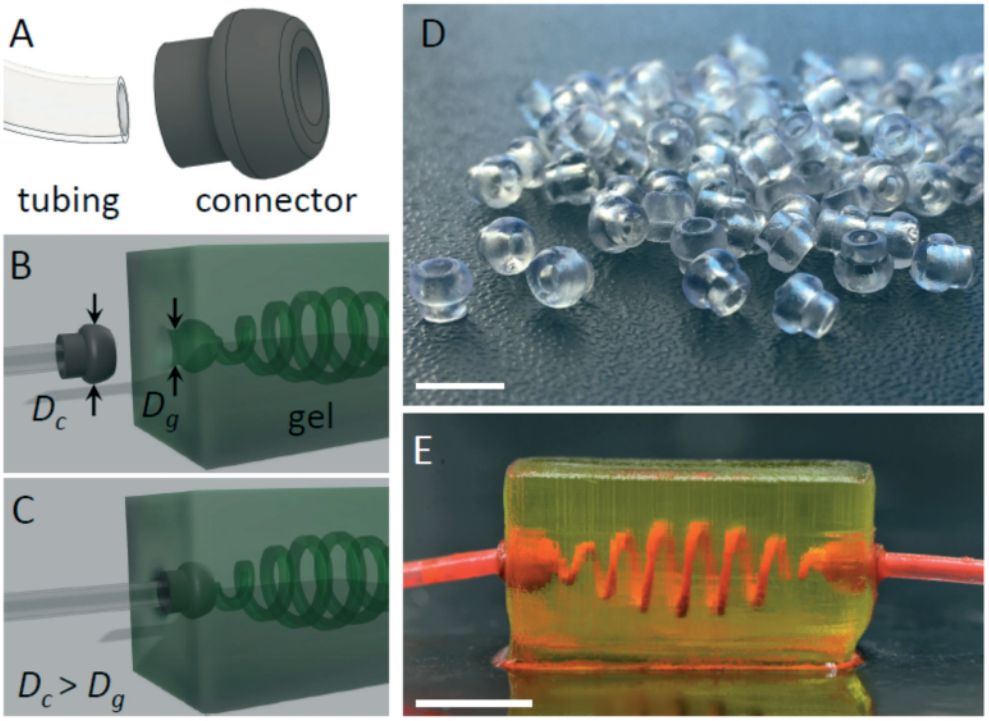

Fig. 2 Plastic 3D printed connector secures fluidic tubing to 3D printed hydrogel. (A) CAD rendering of connector design. (B and C) Illustrations of connector insertion into 3D printed socket opening into a hydrogel channel. For a seal to form, the diameter of the connector head, D_c must be larger than the diameter of the gel socket neck, D_g. (D) Connectors can be rapidly printed and with high fidelity. (E) Connectors secure fluidic tubing to two ends of a 3D printed hydrogel. Channel is filled with an oil-based dye to highlight channel shape. Liquid beneath gel is not leaked oil, but residual water with color reflection from above. Scale bars in (D) and (E) correspond to 5 mm.

can withstand. For these measurements, we fix the gel neck entrance size (D_g = 2.30 mm) and systematically vary the connector head size (2.70 mm $\leq D_c \leq$ 3.50 mm). In this way, we vary the D_c/D_g ratio from 1.17 to 1.52.

To measure the force required for connector insertion as a function of D_c/D_g, we use the normal force sensor of a mechanical rheometer (Fig. 3A). For each measurement, a connector with a defined D_c is mounted on the upper rheometer plate and brought down towards the gel at a fixed velocity (v = 10 μm s^{-1}). Before the connector and gel come into contact, the normal force F is zero. When the two contact, the normal force jumps, and increases as the connector is forced into the gel socket, deforming the gel. The normal force increases to a maximum, F_{max} and then drops back to a value close to zero as the connector locks into the gel socket. A representative measurement is shown in Fig. 3B. For each D_c, we measure multiple force-displacement curves (n = 3–7) and co-plot these data. We observe that F_{max} increases with increasing D_c (Fig. 3C). For connectors with $D_c > 3.60$ we observe that the gel fractures when the connector is inserted (data not shown). This sets an upper limit for D_c/D_g for this connector geometry and gel formulation.

To understand the forces resisting connector insertion, we convert the measured force to a stress τ by dividing the averaged F_{max} for each D_c by the maximum contact area between the connector and gel (see Methods and ESI†). We then define the maximum gel strain during connector insertion to be $\gamma \approx (D_c - D_g)/D_g$, and plot τ as a function of γ (Fig. 3D). We find that the data is fit well by a straight line, even for large $\gamma > 0.5$. This is consistent with elastic behavior, where $\tau = G_e\gamma$ and G_e is the elastic modulus of the gel.[32] From our fit, we find the elastic modulus to be G_e = 11.6 ± 1.1 kPa. To compare this result from insertion force measurements with bulk measurements, we perform shear rheometry on large hydrogels and find the elastic modulus of the gel to be G_e = 10.7 ± 0.2 kPa (Fig. 3E). This confirms that the gel is deformed elastically for this D_c/D_g range and that the elasticity of the gel resists connector insertion. Here, because there were no device design constraints, the overall dimensions of the hydrogel fluidic device were sized such that the printed socket did not interfere with the macroscale structure or functionality of the gel; however, socket size may become an issue for very small devices. For example, practical considerations like physical handling and insertion of the connector into the socket will limit the smallest connector and socket that can be used. For small socket sizes, the gel lip thickness may also become so thin that it is unable to withstand deformation without gel fracture. Also, in situations where important structural features of the gel device are in close proximity to the socket, gel deformation induced by connector insertion may impact these features.

Next, we test the maximum liquid pressure, P_{max} that the pop-it connections can withstand before connector leakage and expulsion. To apply a well-defined hydrostatic pressure,

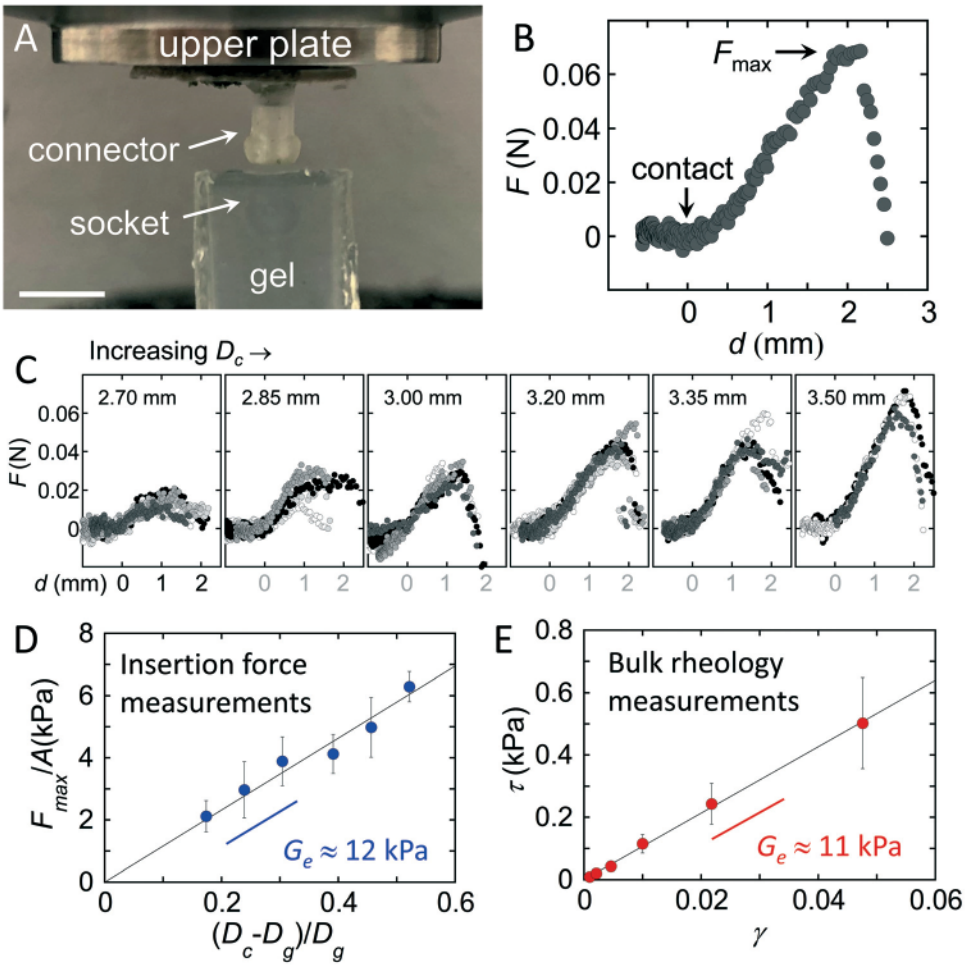

Fig. 3 Connector insertion into gel socket is governed by gel elasticity. (A) Experimental setup for measuring the normal force resisting connector insertion into a gel socket. The upper plate of the rheometer brings the connector down into contact with the gel. The normal force, F is measured by a plate beneath the gel. Scale bar corresponds to 5 mm. (B) Representative plot of normal force F as a function of distance d for the experiment shown in (A) for D_c = 3.50 mm and D_g = 2.15 mm. (C) Force measurements for connectors of varying D_c and gels with fixed D_g = 2.15 mm. F_{max} increases with increasing D_c. Different colored symbols represent measurements on individual gels (n = 3–7 for each D_c). (D) Averaged F_{max} from (C) divided by the contact area A between the connector and gel provides a stress, which is plotted as a function of the maximum dimensionless strain: $(D_c - D_g)/D_g$. The slope of the curve provides the gel elastic modulus G_e. (E) Bulk rheology measurements on the gel provide a comparable value for G_e, confirming the role of gel elasticity.

we attach the pop-it connector to a reservoir of water that can be raised and lowered in a controlled manner (see Methods and ESI†). To apply static pressure without needing to account for pressure loss due to liquid flow, we use hydrogel sockets with a closed inner surface that are not connected to open channels in the gel. For each experiment, we systematically increase the hydrostatic pressure, P, in increments ranging from 0.025 Pa to 10 Pa until connection failure is observed. We do this over the range: $1.16 \leq D_c/D_g \leq 1.67$ by fixing the socket size (D_g = 2.15 mm) and systematically varying D_c. For each connector ratio, we measure P_{max} multiple times ($n \approx 12$) by performing up to 3 repeat measurements on 4 to 5 different hydrogels. Hydrogels are elastically deformed during insertion and removal, and we observe no statistically significant trend in P_{max} with repeated measurements on the same gel. While the gel formulation used in these experiments has a swelling ratio less than 1% in distilled water,[33] we equilibrate the gels for 24 h in distilled water to mitigate any swelling effects.

We find that P_{max} increases with γ, approaching values as high as $P_{max} \approx 3$ kPa (Fig. 4). These pressures are three orders of magnitude greater than those we measure for connector-free couplings ($P_{max} \approx 2.5 \pm 1.5$ Pa, n = 3 hydrogels) and are equivalent to pressures generated in PDMS-based microfluidic devices. Pressure of this magnitude could be used to generate significant flow rates in large channels ($Q \approx 170$ mL min^{-1}, cylindrical channel with D = 0.8 mm and l = 12 mm, see Methods) and are large enough to drive flows through highly vascularized tissues.[34] Interestingly, though both connector insertion and expulsion require gel deformation, P_{max} increases exponentially with γ, while $[F_{max}/A]$ increases linearly with γ (Fig. 3C). This may be because for large D_c the connector head becomes asymmetric along the axis of the cylinder (see images in ESI†); thus, the

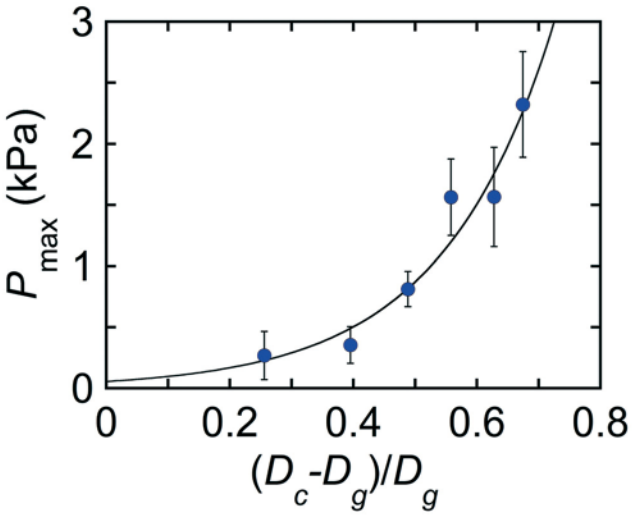

Fig. 4 Seal between connector and gel socket improves as the connector head diameter increases relative to the gel neck diameter. Maximum hydrostatic pressure at failure, P_{max}, plotted as function of maximum gel neck strain during connector expulsion and fit to a simple exponential increase (see Methods). For the connector with the largest head, the connection can withstand pressures $\Delta P > 2.5$ kPa, three orders of magnitude greater than the pressures that standard, connector free approaches can withstand ($\Delta P \approx 1$ Pa).

contact area between the connector and gel during insertion and removal may be quite different. In addition, the gel socket lip is asymmetric and may deform differently during insertion and removal. This apparent hysteresis is supported by preliminary normal force measurements of connector insertion and removal (see ESI†). While understanding this hysteresis is outside the scope of this paper, this warrants further investigation. Here, the liquids we flow through the gel are the same as the liquids used to equilibrate the gel; if liquids with different compositions and osmolalities are used, potential swelling or shrinkage may impact P_{max}.

Pop-it connectors can also be used to connect modular gels to one another. For example, two-sided, dumbbell-shaped connectors (Fig. 5A) matched to 3D printed sockets in opposing gels can be used to bring adjacent gel cubes into contact and hold them in place. For example, joining of two hydrogel cubes using a two-sided connector is shown in a series of images in Fig. 5B and C. To further demonstrate this modularity, we print four hydrogel cubes (edge length, l_c = 9 mm), three of which contain a straight cylindrical channel (D = 1.20 mm) running from one cube face to the opposing face, and one cube with three cylindrical channels running from three different cube faces and joining at a single intersection point. We dye these cubes with food coloring to highlight their individuality, connect them using two-sided pop-it connectors, and drive water through the assembly with one-sided pop-it connectors coupled to microfluidic tubing. Images of the gel modules and the assembly are shown in Fig. 5D and E. The connectors form an excellent seal between hydrogels, allowing for liquid flow. This approach could be used to build complex, reconfigurable hydrogel systems from simple modular components. We note that a variety of connector types exist for connecting modular microfluidic components to one another[35,36] including self-aligning magnetic interconnects[37] and integrated microfabricated gaskets;[38] however, these technologies have not been demonstrated for use with hydrogels.

Pop-it connections offer additional advantages. First, pop-it connections allow for rotation around the long axis of the

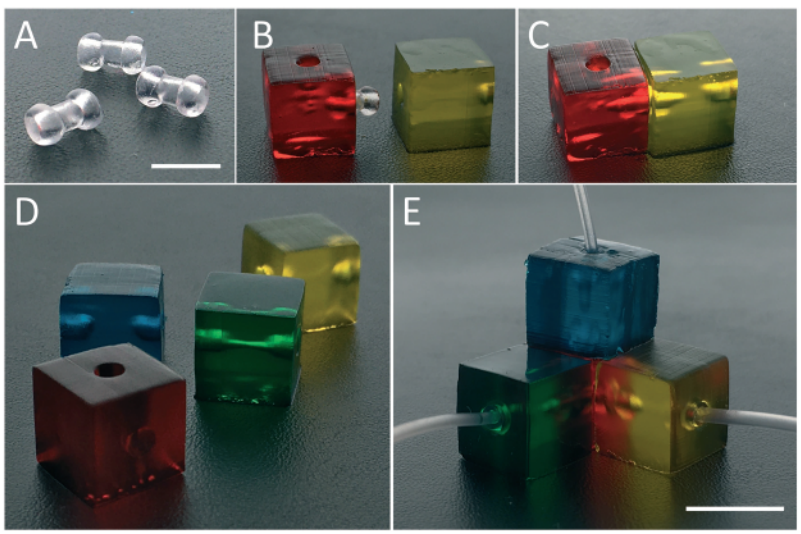

Fig. 5 Double-sided pop-it connectors can be used to build interconnected assemblies from modular gels. (A) Photograph of two-sided connectors. (B and C) Image series of two 3D printed hydrogels joined using a two-sided connector. (D and E) Images of four 3D printed hydrogels joined together using multiple two-sided connectors. Gels were colored with food dye before assembly to illustrate modular nature of the assembly. The blue, green, and yellow cubes contain a single straight channel running from one cube face to another. The red gel contains channels running from three adjacent faces that connect in the center of the cube. The modular assembly does not leak when water is driven through the assembly. Scale bars in (A) and (E) correspond to 5 mm and 10 mm, respectively.

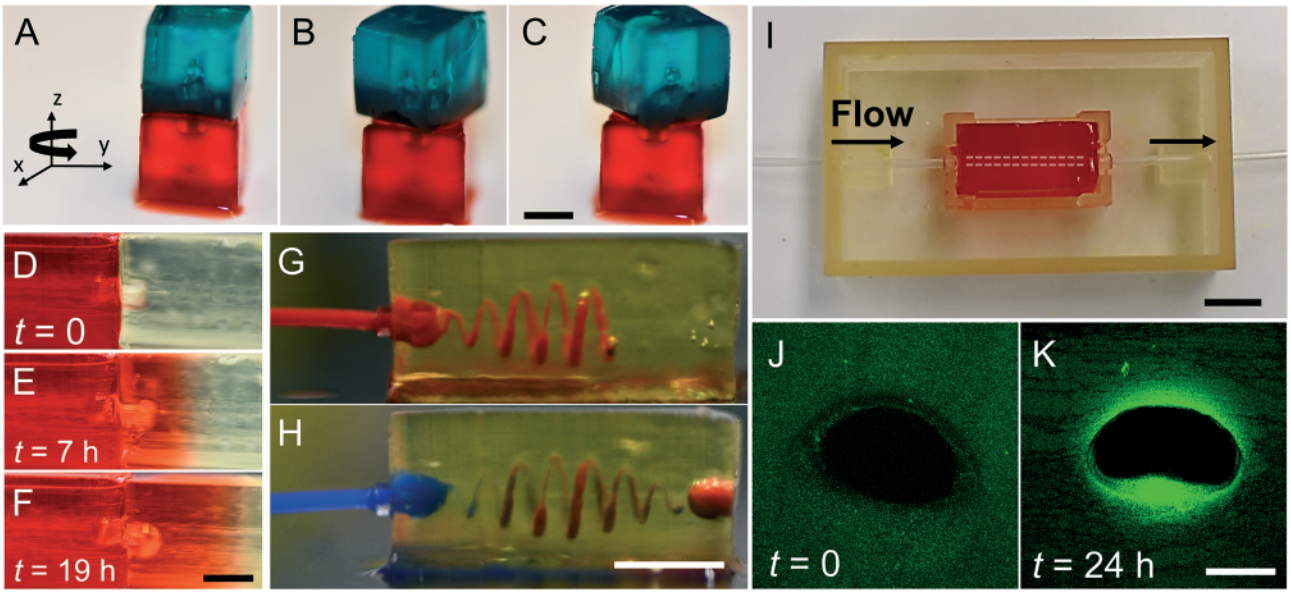

Fig. 6 Pop-it connector advantages and potential applications. (A–C) Connectors allow for free rotation around the long *z*-axis of the connector. The two gels are colored with red and blue food dye for clarity. (D–F) Two hydrogels held in contact by a two-sided connector allows diffusion of material from one gel into the other. Here, red food dye is used. (G and H) Connector reversibility allows multiple fluid streams to be sequentially introduced into the same hydrogel. (I–K) Long-term flow of media through a hydrogel containing bacteria enabled by connectors maintains cell growth and viability, (I) hydrogel and tubing are assembled and held in a plastic 3D-printed holder. Fresh media is driven from left to right through the hydrogel. The gel is dyed red here for clarity. (J and K) Fluorescence confocal microscopy cross-sectional images of gel containing *Pseudomonas aeruginosa* (pMF230; constitutive GFP) before (J) and after (K) growth for 24 hours. Dark center hole is the cross-section of a semi-cylindrical channel ($D \approx 1.20$ mm). Scale bars correspond to: (H) 10 mm; (C), (F), and (H) 5 mm; and (K) 500 μm.

connector. To demonstrate this, we attach two hydrogels together with a two-sided connector and rotate the upper (blue) hydrogel by 45° around the *z*-axis without disturbing the connection (Fig. 6A–C). This rotational degree of freedom could be used for reconfigurable modular assemblies for structure–function studies and soft robotics. Second, two-sided connectors can be used to bring two hydrogel modules into contact to allow for molecular diffusion from one module to another. To demonstrate this, we bring two hydrogel cubes together with a dumbbell shaped connector and observe the diffusion of red dye from one cube into the other (Fig. 6D–F). This could be used to establish well-defined concentration gradients in engineered tissues. Third, the reversibility of the pop-it connection allows one to change the composition of the liquid driven through a given hydrogel during an experiment. To demonstrate this, we introduce one colored oil to a hydrogel module, followed by a second colored oil from a separate tubing source (Fig. 6G and H). This approach could be used to alter the media conditions supplied to living cells embedded in hydrogel. This rapid exchange is not feasible for connections requiring adhesive.[29]

Finally, to demonstrate a clear application of the pop-it connection, we 3D-print a hydrogel cube containing *Pseudomonas aeruginosa* (pMF230; constitutively expressing GFP) with a single straight channel with connection sockets at both ends of the channel and use pop-it connections on either end to establish nutrient flow through the hydrogel. We use a plastic 3D-printed holder to stabilize the gel, connectors, and tubing (Fig. 6I). We store the entire assembly in an incubator at 37 °C and 100% relative humidity and drive tryptic soy broth (TSB) media at a flow rate of 2 mL h^{-1} through the gel. After 24 h, we cross-section the hydrogel and image the GFP intensity with confocal microscopy. A duplicate bacteria-laden hydrogel is cross-sectioned at $t = 0$ and imaged as well for comparison. The images in Fig. 6J and K show clear microbial growth in the hydrogel supplied with media.

The connector design presented here could be modified in a variety of ways. For example, the shape of the connector and socket could be optimized for ease of insertion, for improved seal formation, or to better distribute stress in the hydrogel. Here, we use a bulb-shaped connector, but other connector geometries such as screw shapes and configurations with different rotational and axial symmetry could be explored. In addition, fabrication methods other than 3D printing could be used to structure the connector socket in the hydrogel. For example, a casting approach like that used in soft lithography-based could be used,[39–41] and, the creation of overhanging features in the negative mold could be achieved using two-photon polymerization techniques.[42,43] Pop-it connectors could also be integrated into hybrid hydrogel/PDMS systems.[10] Finally, a wide variety of hydrogel formulations could be explored to improve or optimize connector performance.[44] Gel mechanical properties could be varied by controlling monomer and crosslinker chemistries,[45] molecular weight,[46] gel concentration,[46] and by the addition of filler materials.[47] In addition, alginate,[48] agarose,[48] gelatin methacryloyl (GelMA),[49] poly(vinyl alcohol)

(PVA),[50] and double-network hydrogels with enhanced strength and elasticity[47] could be explored.

Conclusions

In conclusion, the 3D printed "pop-it" connection presented here represents the first reported hydrogel connection mechanism for coupling tubing to hydrogel fluidic devices in a stable, reversible manner to allow for liquid flow. Pop-it connectors mount into well-defined 3D printed sockets by simple insertion and are held in place by the elasticity of the hydrogel, rather than static friction. Using this connection, we show that it is possible to drive fluid flow while sustaining pressures up to $\Delta P \approx 3$ kPa, which is three orders of magnitude greater than the standard connector-free approach and equivalent to the pressures required to drive flow through standard PDMS-based microfluidic devices. We demonstrate that a two-sided connector can be used to couple two hydrogels together to construct modular assemblies with intermodular diffusion. Lastly, we demonstrate that pop-it connectors can be used to establish long-term nutrient flow to hydrogels to sustain the growth and viability of bacteria in the gel. These pop-it connectors will enable a variety of hydrogel applications by allowing for reliable, leak-free flow.

Methods

Hydrogel 3D printing

Hydrogels were designed using CAD software (Autodesk, Fusion 360) and 3D printed using a commercial stereolithography 3D printer (Formlabs, Form 1+). For the aqueous resin formulation, poly(ethylene glycol) diacrylate (PEG-DA) was used as a monomer (10 wt%, Sigma-Aldrich, M_n 700), lithium phenyl-2,4,6-trimethylbenzoylphosphinate (LAP) was used as a photoinitiator (0.1 wt%, Tokyo Chemical Industry), and tartrazine was used as a photoblocker (0.075 wt%, Alfa Aesar). Prepared resin solutions were poured into the printer resin tray. To fabricate gels with well-defined and open structures, resin formulation and light exposure conditions were selected for optimal printing.[11] To ensure adhesion of hydrogel to the print head, microscopy slides (Fisherbrand Colorfrost, 25 mm × 75 mm × 1 mm) were pretreated with Bind-Silane (2.0 vol%, GE Healthcare, 17-1330-01). Microscopy slides were submerged in the Bind-Silane solution for five minutes then baked at 100 °C for another five minutes. Treated slides were attached to the custom-made print head with a UV bonding adhesive (Norland Products).[51] Hydrogel CAD files are available in ESI.† The printing process proceeds by photopolymerizing the object layer-by-layer as described elsewhere.[52]

Connector 3D printing

Connectors were designed using CAD software (Autodesk, Fusion 360) and 3D printed with a commercial stereolithography 3D printer (Formlabs, Form 3) using a methacrylic acid ester-based resin (Formlabs, Clear Resin). After printing, connectors were washed with isopropyl alcohol and post-cured with a benchtop ultraviolet light. Formlabs resins are resistant to ethanol and UV light, both of which can be used for sterilization. As an alternative, Formlabs High-Temperature resin could be used to create autoclavable connectors. Connector CAD files are available in ESI.†

Liquid flow

To drive water through a hydrogel, a plastic syringe (60 mL Soft-Ject Luer Lock, Henke Sass Wolf) was filled with water and mounted into a syringe pump (World Precision Instruments, Model AL-4000). A blunt, 20-gauge dispensing needle was attached to the syringe end with a Luer lock fitting and polyethylene tubing (Scientific Commodities Inc., I.D. = 0.86 mm; O.D. = 1.32 mm). The other end of the tubing, with or without attached pop-it connector, was then inserted into the 3D printed hydrogel. For the hydrogels in Fig. 1 and 2, oil-based red and yellow paint diluted with silicone oil (AR20) was used to highlight the channels.

Hydrostatic pressure measurements

To determine the pressure required for connector failure, we constructed a custom experimental setup capable of applying well-defined hydrostatic pressures (ESI† Fig. S1). The mechanized system consisted of a microcontroller (Elegoo UNO R3), a stepper motor driver (TB6600), and two stepper motors with lead screws (NEMA 17 with 150 mm T8 lead Screws). The lead screws provided controlled linear movement with a minimum step size of 2.5 μm. A water reservoir was mounted to the stepper motor lead screws and connected to the hydrogel through tubing and a pop-it connector. The reservoir was incrementally raised using the stepper motors until the connection between the connector and the hydrogel failed. The height differential between the top of the water reservoir and the pop-it connector was then used to determine the maximum liquid pressure, P_{max} by calculating the hydrostatic pressure at that point using $P_h = \rho g h$, where ρ is density of the fluid, g is gravitational force and h is the height of the fluid. A video of a representative experiment is shown in Video S1.† The data in Fig. 4 is fit to the following function: $\Delta P = ae^{b\gamma}$ where $\gamma \approx (D_c - D_g)/D_g$, $a = 0.056$, and $b = 5.48$.

Flow rate estimates

To estimate the flow rates that our pop-it connections are capable of withstanding, we calculate the volumetric flow rate, Q through a cylindrical channel of diameter, $D = 0.8$ mm and length $l = 12$ mm using the Hagen–Poiseuille equation.

$$Q = \frac{\Delta P \pi D^4}{128 \eta l}$$

Here, η is the dynamic viscosity of the liquid and $\Delta P = \Delta P_{max}$. For water and $\Delta P_{max} = 3$ kPa, we find $Q = 170$ mL min^{-1}.

Rheometry and force measurements

A mechanical rheometer (TA Instruments AR-G2) was used to perform two types of measurements: standard shear rheometry and non-standard normal force measurements. Small amplitude shear rheometry measurements over a range of frequencies, ω = 0.01–1 Hz and strain amplitudes, γ = 0.001–0.05 were performed after mounting coin-shaped 3D-printed hydrogels (sample thickness, h = 3 mm; sample diameter, D_s = 20 mm) in a parallel plate geometry (plate diameter, D_p = 20 mm). Normal force measurements were performed by attaching individual connectors to the upper rheometer head with double-sided adhesive tape. Then, a spot in the center of the lower rheometer plate was marked, 3D printed hydrogel samples were mounted inside a 3D printed housing, and the housing placed on the lower plate in a well-defined position. To further ensure axial alignment of the connector with the socket, the z-position of the upper rheometer head was slowly lowered to approach the hydrogel allowing any necessary adjustments to be made. To measure the normal force required to remove the connector from a hydrogel socket, an inserted connector was retracted by lifting the upper rheometer plate away from the gel. Each measurement took approximately 2–3 minutes in total; if the measurement was prolonged, the hydrogel was kept hydrated by the addition of a small amount of water. The pressure sensing unit of the rheometer is within the lower standing platform. Once the connector and gel are in contact, the integrity of the connector adhesion to the upper geometry should not impact the measurement. If this adhesion were to fail before contact, we would expect a sudden jump in the force. Adhesion of the holder to the lower platform is less likely to fail, would result in a shift in the xy-plane, and would easily be observed by visual inspection.

Measuring contact area of the connector

The contact area, A used in Fig. 3D to calculate τ was estimated using the "Measure" function in Fusion 360. For this, each connector CAD drawing was used to estimate potential contact area of each connector on the inner walls of the hydrogel (See ESI†). Estimating A is done by assuming that the hydrogel socket is stretching into the shape of pop-it connector upon insertion. Also, since the surface area of the pop-it connector acting on the hydrogel during F_{max} should not change for insertion and removal of the connector, the same A values are valid to estimate the pressure acting on the hydrogel during both insertion and removal of the connector.

Growth of 3D printed Bacteria

Pseudomonas aeruginosa (pMF230) is cultured overnight in liquid TSB media with ampicillin (100 μg mL^{-1}). After 12+ h of growth, approximately 10^9 CFU mL^{-1} of planktonic bacteria is added to the bioink resin prior to the 3D printing. The pMF230 strain constitutively expresses GFP, so fluorescence intensity and colony size are used to measure growth and viability. The hydrogel holder in Fig. 6I is 3D printed (Formlabs, Form 3, High Temperature Resin) and autoclaved prior to assembly. After growth for 24 h at 37 °C, the gel is sectioned with a razor blade and imaged with a confocal microscope (Leica SP5; 5× air objective).

Funding

This work was supported by the National Science Foundation (DMR-1455247 and OIA-1736255) and the Army Research Office (W911NF-19-1-0288).

Author contributions

Conceptualization: A. D. B., R. A., and J. N. W.; methodology: R. A., A. D. B., T. B. L., I. J. T., and J. N. W.; investigation: R. A., A. D. B., T. B. L., and I. J. T.; writing – original draft: R. A. and J. N. W.; writing – review & editing: R. A., A. D. B., T. B. L., I. J. T., and J. N. W.; funding acquisition, resources, and supervision: J. N. W.

Conflicts of interest

There are no conflicts to declare.

Acknowledgements

The authors thank Ryan Anderson for help with the derivation of the flow rate expression in the ESI† and Sydney Ross for help with time-lapse imaging. The authors also thank Emmeline and Claire Wilking for assistance with photography.

Notes and references

1 M. Mahinroosta, Z. J. Farsangi, A. Allahverdi and Z. Shakoori, *Mater. Today Chem.*, 2018, **8**, 42–55.
2 H. J. Li, C. Tan and L. Li, *Mater. Des.*, 2018, **159**, 20–38.
3 E. M. Ahmed, *J. Adv. Res.*, 2015, **6**, 105–121.
4 J. Saroia, Y. E. Wang, Q. H. Wei, K. Zhang, T. L. Lu and B. Zhang, *Bio-Des. Manuf.*, 2018, **1**, 265–279.
5 J. M. Rosiak and F. Yoshii, *Nucl. Instrum. Methods Phys. Res., Sect. B*, 1999, **151**, 56–64.
6 J. M. Saul and D. F. Williams, Hydrogels in Regenerative Medicine, *Handbook of Polymer Applications in Medicine and Medical Devices*, ed. K. Modjarrad and S. Ebnesajjad, William Andrew, Oxford, 2014, ch. 12, pp. 279–302.
7 E. Calo and V. V. Khutoryanskiy, *Eur. Polym. J.*, 2015, **65**, 252–267.
8 Q. Y. Chai, Y. Jiao and X. J. Yu, *Gels*, 2017, **3**, 1–15.
9 B. Sidar, B. R. Jenkins, S. Huang, J. R. Spence, S. T. Walk and J. N. Wilking, *Lab Chip*, 2019, **19**, 3552–3562.
10 B. H. Chueh, Y. Zheng, Y. S. Torisawa, A. Y. Hsiao, C. X. Ge, S. Hsiong, N. Huebsch, R. Franceschi, D. J. Mooney and S. Takayama, *Biomed. Microdevices*, 2010, **12**, 145–151.
11 A. D. Benjamin, R. Abbasi, M. Owens, R. J. Olsen, D. J. Walsh, T. B. LeFevre and J. N. Wilking, *Biomed. Phys. Eng. Express*, 2019, **5**, 1–10.
12 B. Grigoryan, S. J. Paulsen, D. C. Corbett, D. W. Sazer, C. L. Fortin, A. J. Zaita, P. T. Greenfield, N. J. Calafat, J. P.

Gounley, A. H. Ta, F. Johansson, A. Randles, J. E. Rosenkrantz, J. D. Louis-Rosenberg, P. A. Galie, K. R. Stevens and J. S. Miller, *Science*, 2019, **364**, 458–464.
13 C. B. Goy, R. E. Chaile and R. E. Madrid, *React. Funct. Polym.*, 2019, **145**, 1–20.
14 Y. F. Zhou, *J. Biomed. Sci.*, 2017, **24**, 1–22.
15 H. J. Koo and O. D. Velev, *Biomicrofluidics*, 2017, **11**, 1–12.
16 C. G. Xia and N. X. Fang, *Biomed. Microdevices*, 2009, **11**, 1309–1315.
17 B. Dhariwala, E. Hunt and T. Boland, *Tissue Eng.*, 2004, **10**, 1316–1322.
18 C. D. Spicer, *Polym. Chem.*, 2020, **11**, 184–219.
19 M. Schaffner, P. A. Ruhs, F. Coulter, S. Kilcher and A. R. Studart, *Sci. Adv.*, 2017, **3**, 1–9.
20 M. Ogawa, K. Higashi and N. Miki, *2015 Transducers - 2015 18th International Conference on Solid-State Sensors, Actuators and Microsystems (Transducers)*, 2015, pp. 1692–1694.
21 L. E. Bertassoni, M. Cecconi, V. Manoharan, M. Nikkhah, J. Hjortnaes, A. L. Cristino, G. Barabaschi, D. Demarchi, M. R. Dokmeci, Y. Z. Yang and A. Khademhosseini, *Lab Chip*, 2014, **14**, 2202–2211.
22 R. Sooppan, S. J. Paulsen, J. Han, A. H. Ta, P. Dinh, A. C. Gaffey, C. Venkataraman, A. Trubelja, G. Hung, J. S. Miller and P. Atluri, *Tissue Eng., Part C*, 2016, **22**, 1–7.
23 I. S. Kinstlinger and J. S. Miller, *Lab Chip*, 2016, **16**, 2025–2043.
24 J. S. Miller, K. R. Stevens, M. T. Yang, B. M. Baker, D. H. T. Nguyen, D. M. Cohen, E. Toro, A. A. Chen, P. A. Galie, X. Yu, R. Chaturvedi, S. N. Bhatia and C. S. Chen, *Nat. Mater.*, 2012, **11**, 768–774.
25 J. Nie, J. Z. Fu and Y. He, *Small*, 2020, **16**, 1–26.
26 A. P. Wong, R. Perez-Castillejos, J. C. Love and G. M. Whitesides, *Biomaterials*, 2008, **29**, 1853–1861.
27 A. M. Christensen, D. A. Chang-Yen and B. K. Gale, *J. Micromech. Microeng.*, 2005, **15**, 928–934.
28 W. J. Chang, D. Akin, M. Sedlak, M. R. Ladisch and R. Bashir, *Biomed. Microdevices*, 2003, **5**, 281–290.
29 S. L. Faley, B. B. Baer, T. S. H. Larsen and L. M. Bellan, *Biomicrofluidics*, 2015, **9**, 1–10.
30 R. Q. Hu, F. Li, J. Q. Lv, Y. He, D. T. Lu, T. Yamada and N. Ono, *Biomed. Microdevices*, 2015, **17**, 1–9.
31 J. N. Patel, B. Kaminska, B. L. Gray and B. D. Gates, *J. Micromech. Microeng.*, 2008, **18**, 1–11.
32 J. R. Ravetz, *Isis*, 1962, **53**, 263–266.
33 B. Yanez-Soto, S. J. Liliensiek, C. J. Murphy and P. F. Nealey, *J. Biomed. Mater. Res., Part A*, 2013, **101**, 1184–1194.
34 R. S. Seymour and A. J. Blaylock, *Physiol. Biochem. Zool.*, 2000, **73**, 389–405.
35 K. C. Bhargava, B. Thompson and N. Malmstadt, *Proc. Natl. Acad. Sci. U. S. A.*, 2014, **111**, 15013–15018.
36 P. Loskill, S. G. Marcus, A. Mathur, W. M. Reese and K. E. Healy, *PLoS One*, 2015, **10**, 1–13.
37 L. J. Y. Ong, T. Ching, L. H. Chong, S. Arora, H. Li, M. Hashimoto, R. DasGupta, P. K. Yuen and Y. C. Toh, *Lab Chip*, 2019, **19**, 2178–2191.
38 S. Miserendino and Y. C. Tai, *Sens. Actuators, A*, 2008, **143**, 7–13.
39 A. W. Justin, R. A. Brooks and A. E. Markaki, *J. R. Soc., Interface*, 2016, **13**, 1–8.
40 A. P. Golden and J. Tien, *Lab Chip*, 2007, **7**, 720–725.
41 J. Nie, Q. Gao, Y. D. Wang, J. H. Zeng, H. M. Zhao, Y. Sun, J. Shen, H. Ramezani, Z. L. Fu, Z. J. Liu, M. X. Xiang, J. Z. Fu, P. Zhao, W. Chen and Y. He, *Small*, 2018, **14**, 1–14.
42 C. N. LaFratta and L. J. Li, *Micro- Nanophotonic Technol.*, 2016, 221–241, DOI: 10.1016/B978-0-323-35321-2.00011-X.
43 C. N. LaFratta, T. Baldacchini, R. A. Farrer, J. T. Fourkas, M. C. Teich, B. E. A. Saleh and M. J. Naughton, *J. Phys. Chem. B*, 2004, **108**, 11256–11258.
44 C. D. Markert, X. Y. Guo, A. Skardal, Z. Wang, S. Bharadwaj, Y. Y. Zhang, K. Bonin and M. Guthold, *J. Mech. Behav. Biomed. Mater.*, 2013, **27**, 115–127.
45 B. D. Fairbanks, M. P. Schwartz, C. N. Bowman and K. S. Anseth, *Biomaterials*, 2009, **30**, 6702–6707.
46 F. Della Sala, M. Biondi, D. Guarnieri, A. Borzacchiello, L. Ambrosio and L. Mayol, *J. Mech. Behav. Biomed. Mater.*, 2020, **110**, 1–9.
47 C. C. Xu, G. H. Dai and Y. Hong, *Acta Biomater.*, 2019, **95**, 50–59.
48 M. Ahearne, Y. Yang, A. J. El Haj, K. Y. Then and K. K. Liu, *J. R. Soc., Interface*, 2005, **2**, 455–463.
49 M. Y. Sun, X. T. Sun, Z. Y. Wang, S. Y. Guo, G. J. Yu and H. Z. Yang, *Polymers*, 2018, **10**, 1–20.
50 J. A. Stammen, S. Williams, D. N. Ku and R. E. Guldberg, *Biomaterials*, 2001, **22**, 799–806.
51 R. Raman, B. Bhaduri, M. Mir, A. Shkumatov, M. K. Lee, G. Popescu, H. Kong and R. Bashir, *Adv. Healthcare Mater.*, 2016, **5**, 610–619.
52 P. F. Jacobs, *Rapid Prototyping & Manufacturing: Fundamentals of Stereolithography*, 1992.

